Journal Name

Dynamic Article Links ►

Cite this: DOI: 10.1039/c0xx00000x

www.rsc.org/xxxxxx

ARTICLE TYPE

Spectroscopy of polycrystalline materials using thinned-substrate planar Goubau line at cryogenic temperatures

Christopher Russell,*[a] Christopher D. Wood,[a] Andrew D. Burnett,[a,b] Lianhe Li,[a] Edmund H. Linfield,[a] A. Giles Davies[a] and John E. Cunningham[a]

Received (in XXX, XXX) Xth XXXXXXXXX 20XX, Accepted Xth XXXXXXXXX 20XX

DOI: 10.1039/b000000x

We investigate the effect of substrate thickness on the transmission bandwidth of on-chip terahertz-frequency-range planar Goubau lines both experimentally and theoretically. The bandwidth and frequency resolution are improved through substrate thinning and geometry modifications (reducing reflections arising from the THz photoconductive generators and detectors). We demonstrate that the enhanced bandwidth (2 THz) and resolution (3.75 GHz) allows this type of on-chip waveguide to be used for spectroscopic measurements of polycrystalline materials from cryogenic (4 K) to room temperature (292 K) by recording vibrational absorption spectra from overlaid samples of lactose monohydrate.

Introduction

Free-space terahertz frequency time-domain spectroscopy (THz-TDS) has been widely used for the spectroscopic study of polycrystalline materials in the frequency range 0.3 – 10 THz, with fingerprint spectra being used to detect and identify different explosives,[1] drugs of abuse,[1] and pharmaceutical compounds,[2] as well as study polymorphic changes in crystalline structures.[2, 3]

However, free space THz-TDS suffers from a diffraction-limited spatial resolution. It also has a limited frequency resolution (typically tens of GHz, set by reflections in the emitter/detector crystals),[4] and generally requires a purged environment to remove atmospheric water vapour from the THz beam-path, which otherwise absorbs strongly.[5] On-chip systems have been developed to address these issues (i.e. removing the need for purging, providing an improved frequency resolution and, by confining the evanescent field to a defined area, improving the spatial resolution).

Of the three more commonly used on-chip geometries (microstrip-line (MSL),[6] coplanar waveguide (CPW)[7] and planar Goubau lines (PGL)), the greater evanescent field extent[8] of PGLs make them better suited for spectroscopic applications owing to stronger interaction with overlaid materials. However, PGLs have so far been limited to a maximum operational frequency of < 800 GHz for a 1-mm-long transmission line.[9] As few spectral resonances are known to occur within this frequency range, these devices have limited application for spectroscopy. Conversely, the increased bandwidth of MSL and CPW devices (~ 1.2 THz and ~ 2 THz, respectively) [6,7] is offset by the limited extent of the associated evanescent field.

Notwithstanding the bandwidth limitations in previous PGL structures, the extensive evanescent field has been used for probing overlaid polycrystalline material and liquid samples guided over the PGL using microfluidics.[10] Similar to CPWs and MSLs, PGL devices are compact, enabling them to be cooled conveniently to cryogenic temperatures for narrow line-width spectroscopic measurements.[11, 12]

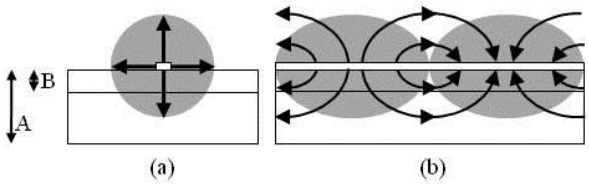

Fig. 1 (a) Cross section of the PGL; the radial electric field pattern is highlighted by vector arrows whose lengths correspond to *r* of equation 2. (b) Electric field pattern along the long axis of the PGL (electric field vectors denoted by arrows; areas of highest electric field magnitude are denoted by the grey cloud). The field lines emerge and terminate on the centre conductor. Substrate thicknesses (A) and (B) correspond to before and after substrate thinning, respectively.

In this letter, we demonstrate how substrate thinning and optimisation of the device geometry can enhance significantly the PGL bandwidth and frequency resolution, allowing this type of on-chip PGL waveguide to be used for practical spectroscopic applications over a wide temperature range (4 – 292 K).

Theory

The propagation of THz radiation along a typical PGL (length 1.5 mm, conductor width 5 µm and 0.5 µm thickness) was simulated using a numerical Maxwell-solver (Ansoft HFSS). This allows the electric field distribution around the waveguide to be calculated, which is necessary to optimise the geometry for spectroscopic applications. The mesh size was set for a convergence frequency of 1.05 THz (the mean mesh element size corresponded to 0.063 × wavelength (λ), where λ corresponds to 1.05 THz), which allows the frequency range 100 GHz – 1 THz

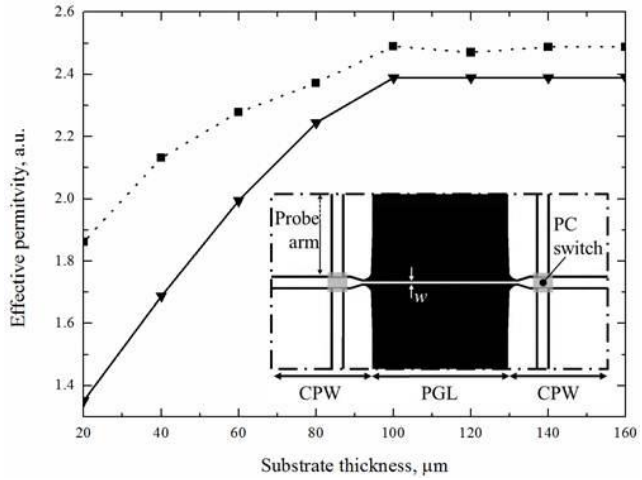

Fig. 2 Main figure: A comparison of the effective permittivity of an unloaded PGL on a quartz substrate as a function of thickness, calculated using HFSS (dashed line) and equation 1 (solid line). Inset: Schematic plan view of the geometry of the active region of the device used, with white areas representing metallization (20/200 nm, Ti/Au) on the (black) quartz substrate; grey areas represent the 350-nm-thick LT-GaAs PC switches; the centre conductor was 1.5 mm long between the PC switches (pair on right labelled) and 5 μm wide (marked *w*) in the PGL section. One of the six 25-mm-long probe arms is indicated.

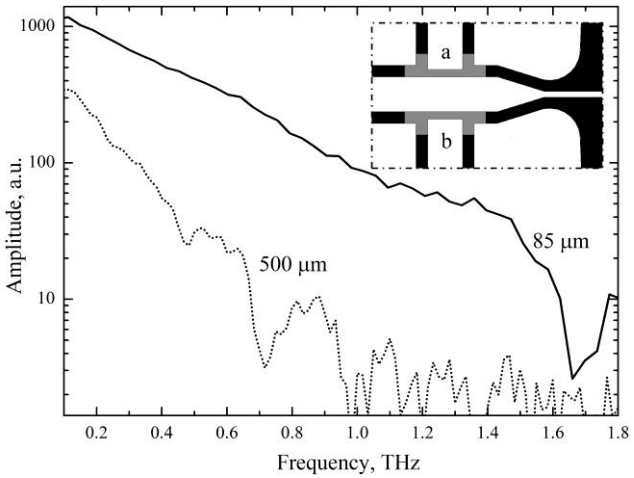

Fig. 3 Main figure: Frequency spectra of unloaded PGLs for two different substrate thicknesses (dotted = 500 μm; solid = 85 μm) showing the increase in bandwidth for thinner substrates. Inset: Magnified schematic plan view of the PC switches and CPW – PGL transition. White areas represent the metallization on the (black) quartz and the (grey) LT-GaAs. The probe arms are labelled a and b. Input pulse measurements are performed by generating with a and detecting with b.

to be modelled. The instantaneous electric field lines were found to be radial along the transmission line (Fig. 1(a)), with the field lines emerging and terminating along the long axis of the PGL conductor (Fig. 1(b)). The magnetic field lines were found to be distributed circularly around the PGL.

A simple analytical model of the effect of substrate thickness can be obtained by assuming that the field lines are perfectly radial, with half of the field lines located above the substrate surface and the remainder below the surface (noting that this assumption is very close to the more precise HFSS simulation results). This allows the effective permittivity of the transmission line to be calculated by taking the average relative permittivity of the area enclosed by the electric field:

$$\varepsilon_{eff} = \frac{\varepsilon_1(\pi+\theta-sin(\theta))+\varepsilon_2(\pi-\theta+sin(\theta))}{\pi r^2} \quad (1)$$

where

$$\theta = 2 * cos^{-1}\left(\frac{h}{r}\right) \quad (2)$$

ε_1 is the relative permittivity of the superstrate, ε_2 is the relative permittivity of the substrate (for quartz ε_2 = 3.78), h is the thickness of the substrate, and r is the radius of the evanescent field. The radius r can be taken as the effective extent of the evanescent field in air, which has been found experimentally to be ~ 100 μm through load testing of quarter wavelength stub filters on PGLs.[9] In Fig. 2, we compare the results obtained by this simple treatment with the more exact numerical simulation results obtained using HFSS. Both sets of results show the expected reduction in effective permittivity of the PGL for substrates thinner than 100 μm (i.e. the expected extent of the evanescent field). The small discrepancy between the two results is likely to be caused by a scaling error introduced by the assumption of a uniform field in the analytical calculation.

Experimental

Experimental results were obtained on identical geometry PGLs. Devices were fabricated on 500-μm-thick, double-side polished quartz, to which a 350-nm-thick low-temperature-grown (LT) GaAs layer was attached using van der Waals bonding.[13] Specifically, LT-GaAs was grown by molecular beam epitaxy at 200 °C, with a 15 minute *ex situ* anneal at 500 °C to increase the device resistivity, and minimise the photocarrier lifetime.[14] The LT-GaAs layer was formed on top of a 100-nm-thick release layer of AlAs, itself grown on a GaAs substrate. Following growth, the LT-GaAs layer, supported by wax, was released from the GaAs substrate by selective etching of the AlAs using dilute (10%) HF acid. The LT-GaAs was then transferred from the etchant solution to the polished surface of a quartz chip using the wax support. The LT-GaAs was left on the substrate for one week to allow van der Waals bonding to attach the LT-GaAs to the substrate (no weight was used to compress the LT-GaAs on the quartz during this process, since previously this was found to lower the device yield by inducing micro-cracking of the LT-GaAs film). The wax was then removed in trichloroethylene, and the LT-GaAs/quartz bond further enhanced in a vacuum oven (15 hours, 30 mbar, 250 ºC). Two 70 μm x 70 μm squares were etched from the LT-GaAs using a H_2SO_4:H_2O_2:H_2O solution (1:8:950 by volume) to define the base material for the THz pulse generation and detection photoconductive (PC) switches (see Fig. 2 inset); the dilute solution produces a sloped side-wall profile in the LT-GaAs, which ensured continuity of metal over-laying the PC switches (formed from 20/200 nm Ti/Au). The PGL geometry consisted of a 1.5-mm-long and 5-μm-wide PGL, with ~ 25-mm-long CPW parasitic arms to remove reflections between the PC switches and the bond-wire contact points. The launch and detection switches were located within the CPW parasitic regions (10 μm gap, 30 μm centre conductor). At the CPW / PGL interface, the CPW centre conductor was tapered

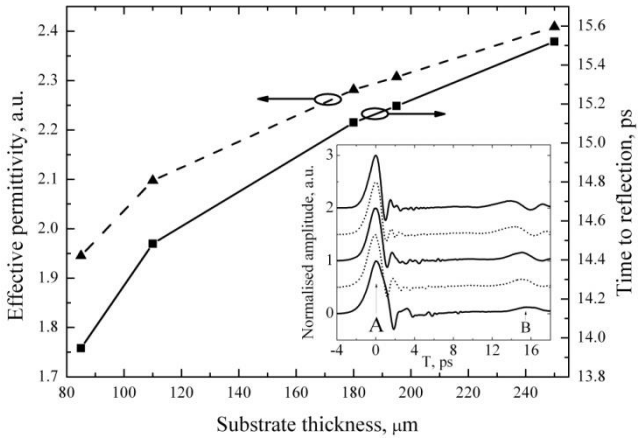

Fig. 4 Main figure: The effective permittivity of the transmission line (left axis) and the time between the main pulse and the reflected pulse arising from etalon effects between the PC switches (right axis) as a function of the substrate thickness, calculated using the time difference between peaks A and B in the time-domain traces (inset). Inset: The normalised amplitude time-domain spectra of the transmitted pulse (with successively thinner substrates being offset vertically by 0.5 units); a main pulse (A: 0 ps) and reflected pulse between the switches (B: 14 – 16 ps) are seen. The main pulse shows a progressive reduction in FWHM with substrate thinning, whilst the separation between peaks A and B reduces, reflecting a reduced effective permittivity and an increased propagation velocity.

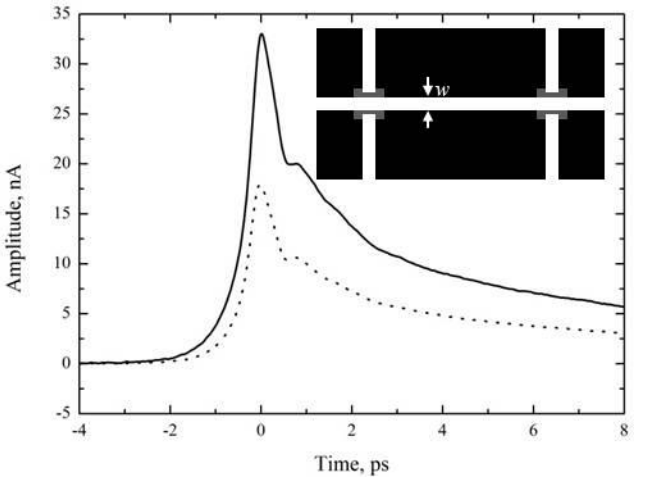

Fig. 5 Main figure: Time domain spectra of the input pulse optically excited from the top of the substrate where the PGL is located (dotted) and through the backside of the substrate (solid line). Inset: Schematic plan view of the geometry of the active region of the PGL device without CPW regions. White areas represent metallization (20/200 nm, Ti/Au), and grey areas representing 350-nm-thick LT-GaAs PC switches; the centre conductor was 1mm long between the PC switches and 30 μm wide (marked *w*) in the PGL section. The device has 11 mm long parasitic probe arms similar to that used in the device shown in the inset of Fig. 2.

down to match the 5 μm wide PGL waveguide, and the ground planes on either side diverged away from the PGL to excite the correct transverse magnetic (TM) mode (inset to Fig. 3). This method of exciting the PGLs with CPWs was originally designed for use with VNAs.[15] The devices were then mounted onto a printed circuit board (PCB) using wax to allow easy removal of the device during subsequent substrate thinning procedures.

For measurement, pulses from a Ti:sapphire laser (100 fs duration, 790 nm centre wavelength, 80 MHz repetition rate and 10 mW average power) were focused onto a 30 V biased PC switch. The generated THz pulse propagated along the PGL to a PC switch located within the second CPW region, onto which an optically delayed and chopped (for lock-in detection) Ti:sapphire laser pulse (average power 10 mW) was focussed, allowing the transmitted 'output' THz pulse to be measured. By varying the optical path length of the delayed Ti:sapphire pulse using a retroflector mounted onto a translation stage, and monitoring the transient current at the second PC switch using lock-in detection, a time-resolved THz pulse signal was recorded. The input pulse generated by the first PC switch was measured by monitoring the adjacent region of the PC switch on the opposite side of the centre conductor, within the same CPW region (see inset Fig. 3). The devices were later removed from the PCB (wax dissolved using trichloroethylene) and mounted onto a lapping chuck, before being thinned using SiC grinding paper (125 μm grit size, Buehler). Each thickness of substrate obtained was measured using a micrometer after lapping, before the substrates were remounted onto the PCB. Repeat measurements of the input and output pulses were thus obtained for a range of substrate thicknesses: 500, 250, 195, 180, 110, and 85 μm.

The results show that, as the substrate is thinned, the FWHM of the input pulse remains unchanged at 1.1 ps, but the amount of dispersion in the transmitted pulse decreases, producing a shorter duration output pulse. We attribute this to the reduction of the mismatch of propagation group velocities above and below the transmission line. The initial substrate thickness (500 μm) produced a FWHM of 1.8 ps, whereas an 85 μm thickness gave 1.1 ps, corresponding to a significant increase in bandwidth of the output pulse from 600 GHz to 1.5 THz, as shown in Fig. 3 (the bandwidth is taken as the point at which the amplitude falls by 98 % in the frequency domain). The corresponding time-domain data shows a secondary peak arising from an etalon effect between the two PC switches (inset to Fig. 4; marked B). If included in the Fourier transform of the time-domain data, the secondary peak introduces etalon oscillations, which interfere with the identification of important spectral features. Therefore, all data was truncated before this secondary peak and then extended with a zero-pad to give a time-domain spectrum made up of 16,384 data points before the Fourier transform was performed.[16] The reflection occurs progressively earlier as the substrate is thinned, owing to the increased group velocity of the pulse, resulting from a reduction in the effective permittivity of the transmission line. This allows the effective permittivity of the transmission line to be calculated using:

$$\varepsilon_{eff} = \left(\frac{ct}{d}\right)^2 \qquad (3)$$

where *c* is the speed of light in vacuum, *d* is the distance travelled by the reflected pulse (3 mm for the 1.5-mm-long PGL), and *t* is the time for the pulse to travel distance, *d*. The variation of effective permittivity with substrate thickness is shown in Fig. 4.

In order to enhance the frequency resolution of the spectra, the CPW regions were removed, and the PGL conductor width made continuous (30 μm), eliminating transmission line impedance mismatches between the PC switches (see Fig. 5 inset). The resulting, 1-mm-long, PGL device supports only the TM PGL mode. The PGL was fabricated on a 500-μm-thick double side polished quartz substrate which was then mechanically thinned using a Logitech PM5 precision polishing and lapping system to a

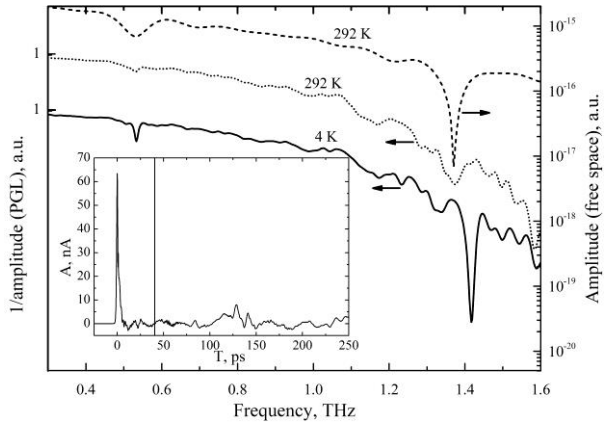

Fig. 6 Main figure: Spectra (21 GHz resolution) of polycrystalline lactose monohydrate at 4 K (solid line) and 292 K (dot) obtained using the PGL, plotted against a reciprocal scale (1/amplitude) for clarity. The same lactose monohydrate sample measured using free space spectroscopy at room temperature is plotted for comparison (dash) on a logarithmic scale. All plots are offset for clarity. Inset: Time-domain data for the transmitted pulse at 4 K with overlaid lactose monohydrate. The vertical line marks the truncation point.

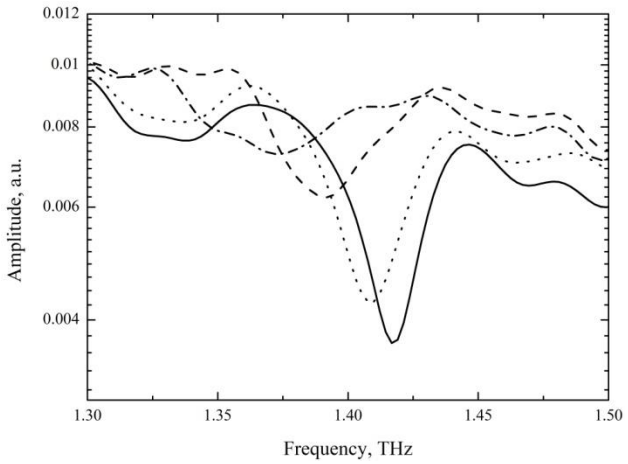

Fig. 7 Spectra (21 GHz resolution) of the peak at ~1.4 THz of polycrystalline lactose monohydrate at four discrete temperatures; 4 K (solid), 100 K (dot), 200 K (dash) and 292 K (dot-dash).

thickness of 50 µm. The polished surface finish on the thinned device facilitates back-side optical excitation of the PC switches, allowing measured samples to cover the PC switches without interfering with THz generation and detection. A comparison between topside and through-substrate laser excitation revealed identical pulse shapes, although the latter excitation technique resulted in higher THz pulse amplitudes (Fig. 5). This amplitude difference is attributed to the gold metallization screening some of the laser power when excited from the PGL side, thus reducing the photocarrier density.

The 50-µm-thick substrate increased further the bandwidth of the PGL device to ~2 THz, and the relative amplitude (per unit length) of the pulse reflection from the PC switches is reduced from 4.56 %/mm to 2.35 %/mm. The reflections arising from the PC switches now have negligible influence on the FFT and hence do not need to be excluded from the time window, in principal increasing the resolution of the spectra to 3.75 GHz. For a noise free spectra (such as that shown in Fig. 6 and Fig. 7), however, the data does need to be truncated (40 ps after the main pulse) to remove transmission line reflections due to corners (radius = 400 µm) and the short probe arms (11 mm), resulting in an overall 21 GHz resolution limit. These issues can be resolved in future devices through using longer probe arms and increasing the corner radii throughout the device geometry. Nevertheless, these observed reflections due to the probe arms do emphasize that the transmission has small attenuation and dispersion.

Having obtained an increase in bandwidth (to 2 THz) by substrate thinning and an improved resolution (3.75 GHz through a geometry change), the PGL was next used for spectroscopic measurements of overlaid polycrystalline materials. A comparison between free space THz-TDS and PGL on-chip spectroscopy was made using lactose monohydrate; 40 mg of lactose monohydrate (Fluka) was pressed into a 0.55-mm-thick pellet (a thickness greater than the extent of the evanescent field above the PGL, to ensure maximum interaction), with a diameter of 8 mm, supported by a copper ring. The sample was measured first using a free space THz-TDS arrangement, in which a Ti:sapphire laser (100 fs duration, 790 nm centre wavelength, 80 MHz repetition rate and 650 mW average power) was used to excite a photoconductive switch comprising semi-insulating GaAs onto which a bowtie antenna was fabricated and biased with a 45 V square-wave modulated signal at a frequency of 10 kHz to allow lock-in detection. The emitted THz radiation was focused by parabolic mirrors onto the pellet. The radiation transmitted through the pellet was collected and focused onto a 2-mm-thick zinc telluride crystal together with a 50 mW optically delayed Ti:sapphire laser probe beam for electro-optic detection.[1] The resulting spectrum is shown in Fig. 6 (dashed line).

The pressed pellet was then removed from the copper ring and diced into 1 mm^2 samples. The samples were placed securely in contact with the PGL, between the PC switches, by placing the sample onto the transmission line and pipetting a DI water droplet onto sample. The water is absorbed by the sample then evaporates away under ambient room conditions leaving the sample firmly attached to the PGL and ensures that the sample is fully in contact. The PC switches, now obstructed by the analyte, were optically excited through the back of the quartz substrate. The PGL was then mounted on the cold finger of a 4 K continuous flow He cryostat with quartz windows for optical access.[17]

The PGL and sample were next cooled to 4 K and spectroscopic measurements were taken after allowing 30 minutes for the temperature to equilibrate. The transmitted pulses were recorded in 10 K increments from 10 K to 100 K, and then in 25 K increments up to room temperature (292 K). The setup was allowed to stabilize for 1.5 hours at each temperature before measurements were recorded. Three scans at each temperature were recorded, truncated and zero padded, before a Fourier transform was performed and the spectra averaged to improve the SNR.[18] The truncated and zero padded data were compared to that of unmodified TDS averaged FFT spectra (3.75 GHz resolution) to reveal low amplitude, high frequency noise with the same strong spectral peaks. The resulting spectra were analyzed by fitting a single Gaussian to each peak in the 3.75 GHz resolution spectra of lactose monohydrate; the data here is fitted without removing a reference signal from the sample signal.

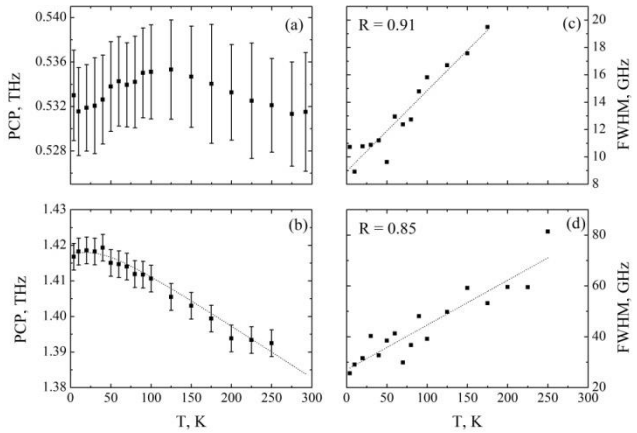

Fig. 8 Peak center position (PCP) as a function of temperature (T) for the (a) 0.5 THz and the (b) 1.4 THz peaks of lactose monohydrate with a line of fit (1.4 THz only, dotted line) using the fit derived from ref [19]. FWHM (determined by Gaussian fit) of the (c) 0.5 THz and (d) 1.4 THz peaks as a function of temperature (T), each with a linear fit and their corresponding R value.

PGL spectroscopy at 292 K of lactose monohydrate reveals two distinct peaks at 0.531 THz and 1.373 THz (Fig. 6). These features correspond well to both experimental (free space and waveguide spectroscopy) and theoretical work.[11, 20, 21] At lower temperatures, the SNR of the TDS spectra increases compared to the room temperature measurements, which we attribute to a reduction in dark current in the PC switches. As the sample is cooled there are also a series of progressive changes in the spectral features as well as a demonstration of the PGLs ability to resolve narrow line-width features (< 10 GHz).

The first peak, centered at 0.531 THz shows no appreciable shift in frequency (Fig 8a) as a function of temperature, whereas the second peak shifts from 1.417 THz (at 4 K) to 1.373 THz (at 292 K) as the temperature is increased (Fig 7 and Fig. 8b), a total change of 34 GHz. This agrees with previous spectroscopic results obtained from polycrystalline materials (fitting parameters from ref. [19]; ν_0 (peak resonance at 0 K) = 1.418 THz, T_c (characteristic temperature) = 140 K, A (equation constant) = 0.15 GHz/K).

$$\nu(T) = \nu_0 - AT_C/\left(e^{T_C/T} - 1\right) \qquad (4)$$

The second peak's center frequencies correspond well to previous experimental work at both temperatures.[21] Both peaks do, however, exhibit the expected peak broadening with increasing temperature, with the first peak broadening by 0.059 GHz/K and the second peak by 0.18 GHz/K (Figs. 8c, d).

Conclusion

In conclusion, we have shown both theoretically and experimentally that lowering the effective permittivity of a PGL, by reducing the substrate thickness, can enhance significantly the bandwidth of the waveguide, owing to a reduction in both the attenuation and dispersion of the pulsed signal. The resolution of the spectra was also enhanced by using a geometry which allowed direct excitation of the PGL TM mode. These changes have increased successfully the PGL bandwidth to 2 THz, with a corresponding spectral resolution of 3.75 GHz, making the PGL a useful spectroscopic tool in the THz regime. This enabled the PGL geometry to be used for variable temperature measurements, which allowed the 0.531 THz peak in polycrystalline lactose-monohydrate to be resolved into a 10 GHz wide peak, demonstrating the PGL's ability to resolve the line-shape and precise frequency of spectral features in overlaid polycrystalline samples. Furthermore, the PGL sensor has allowed tracking of spectral changes (peak position and shape) of a polycrystalline sample as a function of temperature.

Acknowledgements

We acknowledge support from the ESPRC (UK), the Leverhulme Trust, the Royal Society and the Wolfson Foundation, and European Research Council grants 'NOTES' and 'TOSCA'.

Notes and references

[a] *School of Electronic and Electrical Engineering, University of Leeds, Woodhouse Lane, Leeds LS2 9JT, UK, Fax: +44 (0)113 343 7265; Tel: +44 (0)113 343 2015, Email: el06cr@leeds.ac.uk*
[b] *The Faculty of Biological Sciences,University of Leeds, Leeds LS2 9JT, UK*

1. A. G. Davies, A. D. Burnett, F. Wenhui, E. H. Linfield and J. E. Cunningham, *Materials Today*, 2008, **11**, 18-26.
2. J. A. Zeitler, P. F. Taday, D. A. Newnham, M. Pepper, K. C. Gordon and T. Rades, *Journal of Pharmacy and Pharmacology*, 2007, **59**, 209-223.
3. H.-B. Liu and X. C. Zhang, *Chemical Physics Letters*, 2006, **429**, 229-233.
4. Y. C. Shen, P. C. Upadhya, H. E. Beere, E. H. Linfield, A. G. Davies, I. S. Gregory, C. Baker, W. R. Tribe and M. J. Evans, *Applied Physics Letters*, 2004, **85**, 164-166.
5. M. van Exter, C. Fattinger and D. Grischkowsky, *Optics Letters*, 1989, **14**, 1128-1130.
6. M. B. Byrne, J. Cunningham, K. Tych, A. D. Burnett, M. R. Stringer, C. D. Wood, L. Dazhang, M. Lachab, E. H. Linfield and A. G. Davies, *Applied Physics Letters*, 2008, **93**, 182904 (182903 pp.).
7. S. Yanagi, M. Onuma, J. Kitagawa and Y. Kadoya, *Applied Physics Express*, 2008, **1**, 012009 (012003 pp.).
8. L. Dazhang, *Thesis: On-chip terahertz pulsed systems, University of Leeds*, 2010.
9. L. Dazhang, J. Cunningham, M. B. Byrne, S. Khanna, C. D. Wood, A. D. Burnett, S. M. Ershad, E. H. Linfield and A. G. Davies, *Applied Physics Letters*, 2009, **95**, 092903 (092903 pp.).
10. S. Laurette, A. Treizebre and B. Bocquet, *Journal of Micromechanics and Microengineering*, 2011, **21**, 065029.
11. E. R. Brown, J. E. Bjarnason, A. M. Fedor and T. M. Korter, *Applied Physics Letters*, 2007, **90**, 061908.
12. M. Walther, B. M. Fischer and P. Uhd Jepsen, *Chemical Physics*, 2003, **288**, 261-268.
13. J. Cunningham, C. Wood, A. G. Davies, I. Hunter, E. H. Linfield and H. E. Beere, *Applied Physics Letters*, 2005, **86**, 1-3.
14. I. S. Gregory, C. Baker, W. R. Tribe, M. J. Evans, H. E. Beere, E. H. Linfield, A. G. Davies and M. Missous, *Applied Physics Letters*, 2003, **83**, 4199-4201.
15. T. Akalin, A. Treizebre and B. Bocquet, *IEEE Transactions on Microwave Theory and Techniques*, 2006, **54**, 2762-2767.

16. M. Naftaly and R. E. Miles, *Optics Communications*, 2007, **280**, 291-295.
17. C. Wood, J. Cunningham, P. C. Upadhya, E. H. Linfield, I. C. Hunter, A. G. Davies and M. Missous, *Applied Physics Letters*, 2006, **88**, 142103-142101.
18. J. S. Melinger, S. S. Harsha, N. Laman and D. Grischkowsky, *J. Opt. Soc. Am. B*, 2009, **26**, A79-A89.
19. Y. C. Shen, P. C. Upadhya, E. H. Linfield and A. G. Davies, *Applied Physics Letters*, 2003, **82**, 2350-2352.
20. D. G. Allis, A. M. Fedor, T. M. Korter, J. E. Bjarnason and E. R. Brown, *Chemical Physics Letters*, 2007, **440**, 203-209.
21. S. Saito, T. M. Inerbaev, H. Mizuseki, N. Igarashi, R. Note and Y. Kawazoe, *Japanese Journal of Applied Physics* 2006, **45**, L1156-L1158.